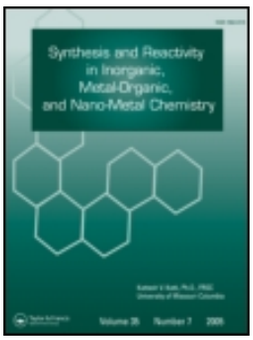

Taylor & Francis
Taylor & Francis Group

Synthesis and Reactivity in Inorganic, Metal-Organic, and Nano-Metal Chemistry

ISSN: 1553-3174 (Print) 1553-3182 (Online) Journal homepage: https://www.tandfonline.com/loi/lsrt20

A Study on Corrosion Behavior of Electrodeposited Zn-Rutile TiO_2 Composite Coatings

M. K. Punith Kumar , T. V. Venkatesha , M. K. Pavithra & A. Nithyananda Shetty

To cite this article: M. K. Punith Kumar , T. V. Venkatesha , M. K. Pavithra & A. Nithyananda Shetty (2012) A Study on Corrosion Behavior of Electrodeposited Zn-Rutile TiO_2 Composite Coatings, Synthesis and Reactivity in Inorganic, Metal-Organic, and Nano-Metal Chemistry, 42:10, 1426-1434, DOI: 10.1080/15533174.2012.682684

To link to this article: https://doi.org/10.1080/15533174.2012.682684

Synthesis and Reactivity in Inorganic, Metal-Organic, and Nano-Metal Chemistry, 42:1426–1434, 2012

ISSN: 1553-3174 print / 1553-3182 online
DOI: 10.1080/15533174.2012.682684

Taylor & Francis
Taylor & Francis Group

A Study on Corrosion Behavior of Electrodeposited Zn-Rutile TiO_2 Composite Coatings

M. K. Punith Kumar,[1] T. V. Venkatesha,[1] M. K. Pavithra,[1] and A. Nithyananda Shetty[2]

[1]*Department of PG Studies & Research in Chemistry, Kuvempu University, Shankaraghatta, India*
[2]*Department of Chemistry, National Institute of Technology Karnataka, Surathkal, India*

The Zn and Zn-TiO_2 composite coatings were fabricated by electrolyzing respective plating solutions of Zn and Zn-TiO_2. The rutile TiO_2 nanoparticles (size ≤100nm) were used for the preparation of composite coatings. The corrosion behavior of the deposits was examined by electrochemical methods. The anticorrosive property of coatings was supported by measuring their corrosion potential, polarization resistance, charge transfer characteristic peak and break frequency. The surface morphology of deposits was studied by scanning electron microscopy, energy-dispersive X-ray diffraction spectroscopy, and X-ray diffraction techniques. The change in morphology of Zn-TiO_2 composite with respect to Zn is correlated with their corrosion behavior.

Keywords composite coating, corrosion, EIS, electrodeposition, Zn-TiO_2

INTRODUCTION

Zinc deposition is one of the widely used surface finishing processes in industries. It is used as a sacrificial coating to protect steel from corrosion. However, the life span of zinc coatings is limited due its rapid dissolution in aggressive environment.[1] Hence many efforts have been focused on improving the properties of zinc coatings by codeposition with various micro- or nanosized particles. In recent years nanoparticles are employed largely instead of microparticles in composite coating because of their advantageous properties along with their easy availability.

The metal-particles composites can be fabricated by various methods. Among them electrodeposition is one of the best methods, which has the advantages of low cost, room temperature, single step, good reproducibility, controllable electrochemical parameters, and reduction of waste.[2–4] Using an electrodeposition technique, a variety of nanosized particles such as ZrO_2,[5] TiO_2,[6] and NiO[7] have been successfully incorporated in to zinc deposits. The inclusion of these nanoparticles makes the deposit to possess better physical, mechanical, and electrochemical properties of zinc electrodeposit.

Particularly, TiO_2 nanoparticles are in great demand for the generation of composite metal coatings because they impart properties such as corrosion resistance, semiconducting, photocatalytic, wear, and photo-induced biocidal effect.[6,8–12] Many researchers have reported different methods for the generation of Zn-TiO_2 composite coating. Among them few results were reported on fabrication and corrosion behavior of Zn-TiO_2 composite coatings obtained from different type and sized TiO_2 nanoparticles. Vlasa et al. reported the corrosion behavior of Zn-TiO_2 composites by taking 32 nm Anatase and Degussa TiO_2 nanoparticles.[8] Yang et al. studied the corrosion behavior of sealed Zn-TiO_2 composite coatings produced on NdFeB magnet[13] and Gomes et al. fabricated Zn-TiO_2 composite coatings on mild steel by pulsed electrodeposition method and they have studied corrosion behavior of pulse deposited Zn-TiO_2 composite coating.[14] Also, in our previous work we generated and studied the corrosion behavior of Zn-TiO_2 composite coating using a single concentration of TiO_2 particles.[6]

However, even in the same experimental conditions coatings obtained from different types of nanoparticles shows different properties because of the different size, crystalline structure, and surface properties of the nanoparticles.[8] Hence there is further scope to generate the Zn-TiO_2 composite coatings of desired properties by using different TiO_2 nanoparticles.

The main objective of this work is to fabricate the Zn-TiO_2 composite films on steel substrate from solutions containing different concentrations of ≤100 nm–sized rutile TiO_2 nanoparticles and to investigate the influence of TiO_2 nanoparticles on the corrosion resistance and morphology of Zn coating. The results of electrochemical measurements (i.e., Tafel) and Electrochemical Impedance Studies (EIS) were correlated with those obtained by using nonelectrochemical methods such as scanning electron microscopy (SEM), energy-dispersive X-ray diffraction spectroscopy (EDS), and X-ray diffraction (XRD) techniques.

Received 6 August 2011; accepted 25 March 2012.
Address correspondence to T. V. Venkatesha, Department of PG Studies & Research in Chemistry, Kuvempu University, Shankaraghatta 577 451, India. E-mail: drtvvenkatesha@yahoo.co.uk

EXPERIMENTAL

Preparation of Zn and Zn-TiO_2 Composite Coating

The electrodeposition method was used to fabricate Zn and Zn-TiO_2 composite coatings in a conventional two-electrode cell. The zinc plate (99.999%) and mild steel (AISI 1079, composition C = 0.5, Mn = 0.5%, S = 0.005%, and Fe = 98.95%) were used as anode and cathode, respectively, with an exposed surface area of 4 × 4 cm^2. Before plating, the zinc plate surface was activated by dipping it in 5% HCl for few seconds followed by water wash. The steel surface was ground with different grit waterproof abrasive paper and then degreased with trichloroethylene degreaser plant and pickled in 10% HCl followed by water wash.

The plating solutions used for coating process were made of composition in Table 1 with or without TiO_2 nanoparticles at 25 ± 2°C. For the present work rutile TiO_2 nanoparticles of size ≤100 nm (637262-25G: MKBB7074) purchased from sigma Aldrich, India and other chemicals of analytical grade purchased from Hi Media India were used.

In the present work the plating solutions to generate Zn-TiO_2 composite coating were prepared by adding 2, 6, and 10 g/L of the previously mentioned TiO_2 particles and were agitated for 24 h by means of stirring using magnetic stirrer (Remi make, India) to ensure uniform dispersion of nanoparticles in plating solution. The Zn and Zn-TiO_2 electrodeposits were prepared by applying DC current for 10 min with a current density of 0.03 Acm^2 at stirring speed of 400 rpm at room temperature (25 ± 2°C). So obtained coatings were named as D_0 (Zn + 0 g/L TiO_2), D_1 (Zn + 2 g/L TiO_2), D_2 (Zn + 6 g/L TiO_2), and D_3 (Zn + 10 g/L TiO_2).

Electrochemical Tests

The electrochemical corrosion studies were performed in a conventional three-electrode glass cell by using CHI 660C electrochemical workstation (U.S. make) at 25 ± 2°C. The 0.25 gL^{-1} of aerated ammonium sulfate solution was used as corrosive media. A saturated calomel electrode (SCE) and a platinum wire served as the reference electrode and counterelectrode, respectively. The coated specimens were used as working electrode with 1 cm^2 exposure area and were immersed in the corrosive media for about 1 hr before polarization and impedance measurements to ascertain the steady state potential or open circuit potential (OCP).

TABLE 1
Optimized bath composition and operating parameters for zinc deposition

Bath composition	Concentration	Operating conditions
$ZnSO_4$	180 g/L	Anode: Zinc plate (99.99% pure)
Na_2SO_4	30 g/L	Cathode: Mild steel plate
NaCl	10 g/L	Current density: 0.03 A cm^{-2}
SLS (sodium lauryl sulfate)	1.5 mM	Plating time: 10 min
		Stirring speed: 400 rpm
		pH: 2.5 Temperature: 27 ± 2°C

EIS measurements were conducted discontinuously during 72-h immersion with an alternating current signal of frequency range from 100 kHz to 10 mHz at 6 points per decade frequency with sinusoidal signal amplitude of 5 mV. The measured EIS data were curve fitted and analyzed with the help of commercial ZSimpWin 3.21 software to obtain impedance parameter. Each experiment was repeated thrice to confirm reproducibility of the results.

Surface Characterization

The surface morphology of the coating was investigated using JOEL–JEM–1200–EX II SEM and the TiO_2 particle content in the coated film was determined by EDS analysis coupled with SEM. XRD analysis of electrodeposits was carried out using Philips TW3710 X-ray diffractometer (Indian Institute of Science, Bangalore, India) with Cu Kα radiation ($\lambda = 0.1540$ nm) working at 30 mA and 40kV.

RESULTS AND DISCUSSION

Tafel Polarization

For polarization studies the working electrode was either of pure Zn coating or any one of the composite coating and platinum wire served as counterelectrode. The polarization curves obtained for the Zn and Zn-TiO_2 composite coatings in 0.25 g/L of ammonium sulfate solution are depicted in Figure 1. All polarization results were measured at their OCP of respective coatings and the corrosion kinetic parameters were obtained with reference to saturated calomel electrode and are tabulated in Table 2.

The corrosion potentials of Zn-TiO_2 composite coatings are less negative than pure Zn. This evidences the noble character

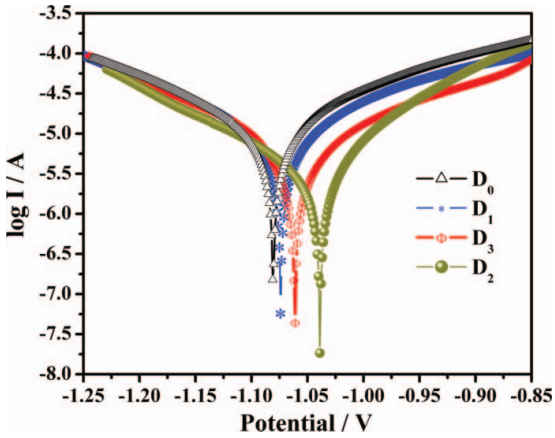

FIG. 1. Potentiodynamic polarization curves for Zn coating D_0 and Zn-TiO_2 composite Coatings D_1, D_2, and D_3 (color figure available online).

TABLE 2
Electrochemical parameters estimated from potentiodynamic polarization curves

Specimen	E_{corr} V	I_{corr} in μA cm^{-2}	β_c mV dec^{-1}	β_a mV dec^{-1}	Corrosion rate $\mu g\ h^{-1}$
D_0	−1.081	14.36	154.34	171.28	16.98
D_1	−1.061	7.37	163.98	171.40	8.716
D_2	−1.039	4.303	150.62	116.21	5.089
D_3	−1.074	12.69	175.56	171.90	15.01

of Zn-TiO_2 composites. The corrosion current density for pure zinc coating is 14.36 μA, where as for D_1, D_2, and D_3 coatings are 7.37 μA, 4.30 μA, and 12.69 μA. The coating D_2 possess lowest i_{corr} value than other two composite coatings D_1 and D_3. The lowest i_{corr} of D_2 is due to the incorporation of TiO_2 nanoparticles with zinc matrix, where the incorporated TiO_2 particles decreases the active surface area or anodic sites in zinc coating, which are responsible for corrosion.

However, the composite coating D_3 obtained from solution of higher concentration of TiO_2 (10 g/L) exhibited less E_{corr} and high i_{corr} value than that of other two composite coatings D_1 and D_2. But compared to pure zinc coating the D_3 exhibits appreciable corrosion resistance. This higher i_{corr} and more negative E_{corr} of D_3 could suggest an acceleration of the corrosion process, which may be due to chemical heterogeneities generated in the zinc matrix by the incorporation of agglomerated TiO_2 particles.

The anodic and cathodic Tafel slope values of Zn-TiO_2 composite coatings are different from pure Zn coating, which indicates the influence of TiO_2 inclusion on the kinetics of both cathodic and anodic reactions of Zn coating. And also improved anticorrosion property of composite coating was confirmed by E_{corr} and i_{corr} data.

EIS Analysis

The EIS measurements provide insight in to the characteristics and kinetics of electrochemical process occurring at the electrode/solution interface in corrosive media or it is capable of *in situ* and nondestructively probing relaxation phenomena over a wide frequency range. The electrochemical impedance measurements were carried out for all coatings at their OCP in the frequency range 100 kHz to 10 mHz.

The measured EIS data are presented as Nyquist plots and typical Bode plots. EIS measurements after 1 h immersion of samples in 0.25 g/L of ammonium sulfate solution shows coating obtained from 6 g/L of rutile TiO_2 nanoparticles (D_2) has higher impedance modulus than other coatings. Further EIS measurement was carried at 4, 24, 48, and 72 h to know the anticorrosion behavior of coatings that are immersed in corrosive media.

The Nyquist plots in Figure 2 correspond to D_0, D_1, D_2, and D_3 coatings, which were exposed to corrosive media at different immersion time. The Nyquist plots show that all the coatings exhibited three capacitive loops at all immersion time, but the magnitude of third capacitive loop is smaller for the 1 and 4 h immersion time and it is much more intense and distinguishable at the 24, 48, and 72 h immersion times. Moreover these capacitive loops are well resolved in Bode plots.

The analysis of shape of the impedance spectra with the fitted electrical equivalent circuit (EEC) help to understand the electrochemical process occurring at the surface. This means that obtaining a good fit does not imply that the used model is correct. However, the shape of the spectra is influenced by electrochemical process at the surface and/or by the geometric factors of electrode.[15] Hence to obtain impedance parameters the experimentally determined EIS data were fitted with suitable equivalent circuit (which possess lower percentage of error) with the help of ZSimpWin 3.21 software.

The EEC with 3RC couples of Figure 3 was used to fit the impedance data. To get appreciable fitting results the employed low frequency capacitance element (C) in EEC was replaced by constant phase element (CPE). The impedance of CPE is defined by the following equation:

$$Z(jw) = (Q)^{-1}\ (jw)^n \qquad [1]$$

where Q = CPE constant, j = imaginary unit, w = angular frequency ($w = 2\pi f$; f = frequency), and n = CPE exponent ($-1 \geq n \leq 1$).

The CPE exponent n is a measure of capacitance dispersion, for an ideal capacitor n = 1 and if there is decrease in the n value it means the nonuniform distribution of current arises from the surface roughness and surface defects.[16–19]

In the circuit (Figure 3) each element is attributed to the following contributions.[8,20–22] First, R_e is the electrolyte resistance appeared between the reference electrode and the surface of the coated specimen (i.e., working electrode). Second, the high-frequency contribution ($C_f - R_f$) is ascribed to the dielectric character of the thin surface layer formed from the corrosion products (C_f) and its electrical leakage from ionic conduction through its pores (R_f). Third, the medium-frequency contribution is attributed to the double layer capacitance (C_{dl}) at the electrolyte/coated surface (Zn and Zn-TiO_2) interface at the bottom of the pores coupled with the charge transfer resistance (R_{ct}). This charge transfer resistance is closely related to corrosion rate. Fourth, the low-frequency couples ($Q_F - R_F$) may related to a redox process taking place at the surface likely involving the thin layer of corrosion products accumulated at the electrolyte/working electrode interface.

The calculated impedance data from the equivalent circuit approaches the experimental data of Zn coating in presence and absence of TiO_2 particles in the bath solution. The obtained electrochemical parameters are presented in Table 3. In the initial measurements the magnitude of low-frequency capacitive loop is less because there is no considerable corrosion products on the electrode and hence the obtained impedance response is purely

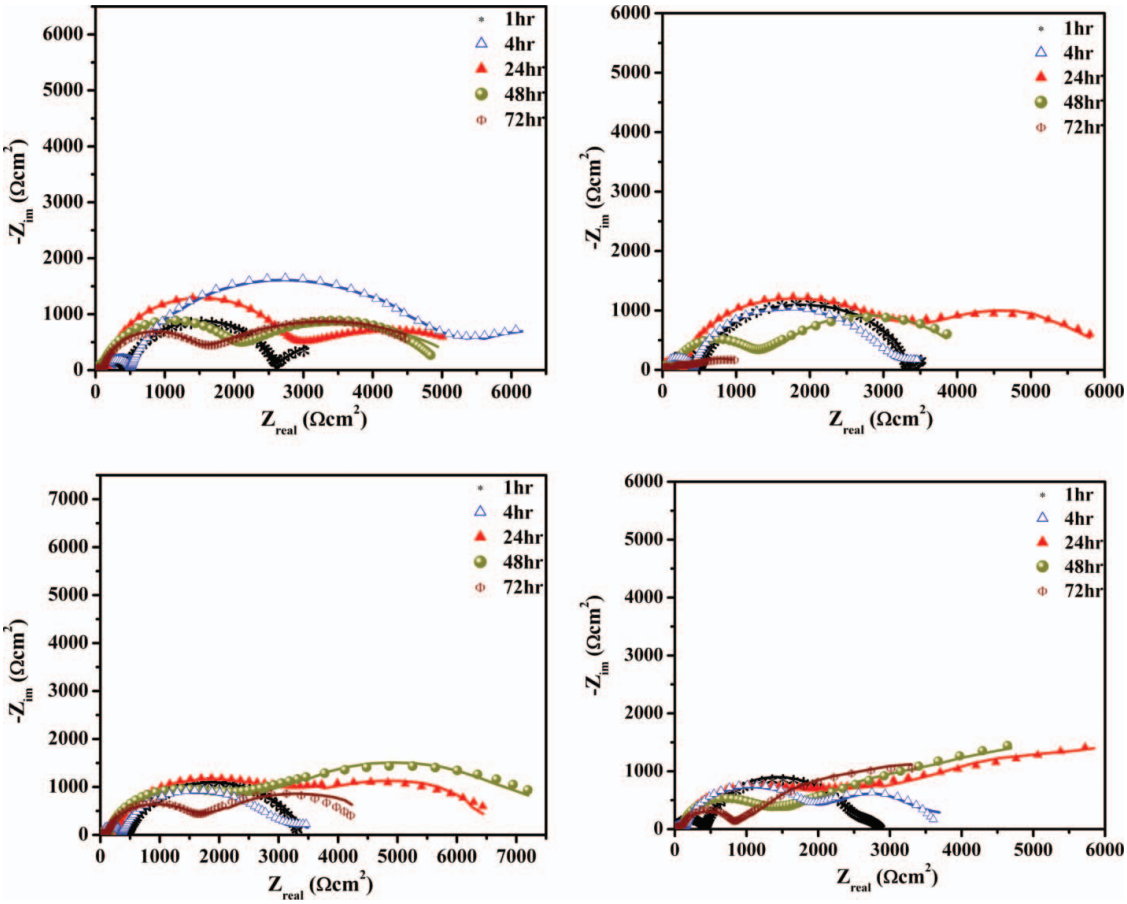

FIG. 2. Experimental (–) and simulated (symbol) Nyquist plots of Zn coating D_0 and Zn-TiO_2 composite coatings D_1, D_2, and D_3 (color figure available online).

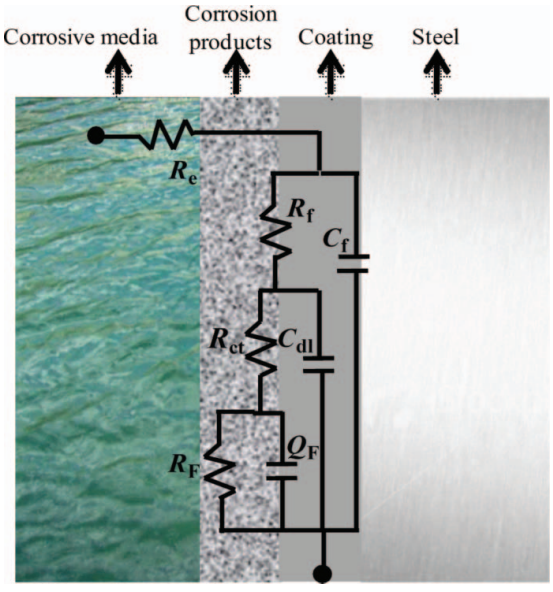

FIG. 3. Electrical equivalent circuit used for simulation of EIS data of Zn coating and Zn-TiO_2 composite coatings (color figure available online).

due to coated surface. As a result maximum coating resistance (R_f) with minimum capacitance (C_f) was observed. The high-frequency response elements C_f and R_f are due to the dielectric behavior of corrosion products layer formed on the electrode after 4 h of immersion. According to data as time proceeds R_f value varied with lesser C_f, which may be due to ionic conduction through the layer. This infers the semipermeable nature of the corrosion product layer. The formed semipermeable layer decreases the electroactive area and it is confirmed by middle- and low-frequency impedance response.

With increase in the immersion time the adherent corrosion products layer formed provides a barrier for direct contact between corrosive media and active electrode surface. As a result the double layer capacitance C_{dl} decreased with time. The charge transfer resistance R_{ct} was slightly varied through different measurements at different immersion time. This arises due to variation in the thickness of corrosion products layer and due to this variation, the low-frequency response elements Q_F and R_F also slightly disturbed. The decrease in low-frequency CPE exponent (n_F) (Table 3) confirms the presence of adhered corrosion products because low-frequency response purely depends on this nonuniform, rough corrosion products layer.

TABLE 3
Electrochemical parameters determined by electrical equivalent circuit simulation

Specimen	Time (h)	C_f in nFcm^{-2}	R_f in Ωcm^2	C_{dl} in μFcm^{-2}	R_{ct} in Ωcm^2	Q_F in 10^{-6} (Ω^{-1}cm^{-2}S^{-n})	n_F	R_F in Ωcm^2	$^*R_p$ in Ωcm^2	%Error
D_0	1	6.463	448	15.17	2163	110.7	0.89	396	3007	1.34
	4	10.09	504	10.59	4845	183	0.76	715	6064	1.32
	24	119	169	3.298	2829	516.3	0.50	2008	5006	0.92
	48	314.5	81	1.421	2044	240.2	0.56	2709	4834	1.27
	72	153.1	113	3.712	1563	386.4	0.57	2796	4472	1.6
D_1	1	4.52	467	19.10	2868	9.11	0.86	92	3427	1.38
	4	6.56	419	9.679	2868	35.74	0.8	165	3452	1.80
	24	14.4	276	6.328	3029	340.6	0.58	2498	5803	2.21
	48	31.06	171	4.46	1113	448	0.63	2552	3836	1.36
	72	51.16	129	30.9	183	1315	0.54	664	976	1.53
D_2	1	4.99	451	23.91	2326	45.99	0.98	684	3461	1.90
	4	8.37	330	11.52	2850	354.5	0.8	310	3490	2.15
	24	17.9	228	4.943	3012	192.1	0.51	3194	6434	1.51
	48	36.63	153	2.404	2037	154.4	0.51	5001	7191	1.48
	72	60.81	117	2.94	1531	329.2	0.40	2564	4212	2.31
D_3	1	32.77	420	13.59	2155	247.8	0.78	289	2864	1.48
	4	39.48	144	4.635	1793	379.1	0.59	1668	3605	1.65
	24	58.9	125	2.241	1860	242.2	0.58	3736	5721	2.28
	48	84.09	103	0.878	1282	404.9	0.41	3253	4638	2.14
	72	118.8	90	1.37	749	652.8	0.51	2469	3308	0.88

However, after 4 h immersion time the R_f and R_{ct} values decreased whereas a higher R_F value was noticed. Meanwhile, R_P represents the combination of R_f, R_{ct}, and R_F and is closely related to the corrosion rate of the material.[20,23] Hence, higher R_p values for longer immersion time show the appreciable anticorrosive nature of coatings.

All coatings D_0, D_1, D_2, and D_3 showed higher polarization resistance [$R_p = (R_f + R_{ct} + R_F)$] at 24, 48, and 72 h of immersion. The impedance parameters presented in Table 3 and complex EIS plots reveals that the Zn-TiO_2 composite coatings have higher anticorrosive property except D_1. In composite coating D_1, the R_p value drastically decreases after 24 h of immersion time. But, the composite coating produced by 6 g/L of TiO_2 particles exhibited higher R_p values with high charge transfer resistance than other coatings in EIS measurements. But the Zn-TiO_2 coating obtained from higher concentration of TiO_2 (10 g/L) D_3 and lower concentration of TiO_2 (2 g/L) D_1 shows less R_p value than D_2 composite coatings. This may be due to defects formed due to the nonuniform distribution of TiO_2 particles in the deposit. However, TiO_2 incorporated Zn coatings are superior in their anticorrosive behavior than Zn coating.

Analysis of Bode Plots

The Bode plots (i.e., log|Z| and phase angle (θ) as a function of frequency) are more informative in the coatings corrosion analysis. The Bode plot depicted in Figure 4 corresponds to Zn-TiO_2 composite coating D_2. The absolute impedance value |Z| for all the deposits is at a minimum in the 1 and 4 h immersion periods except D_0, but increased for immersion at 24, 48, and 72 h and it is given in Figure 5. The results obtained from Bode plots are well matched with those from Nyquist plots. The Zn-TiO_2 composite coating fabricated from 6 g/L of TiO_2 particles shows maximum impedance value up to 72 h immersion period when compared with other coatings.

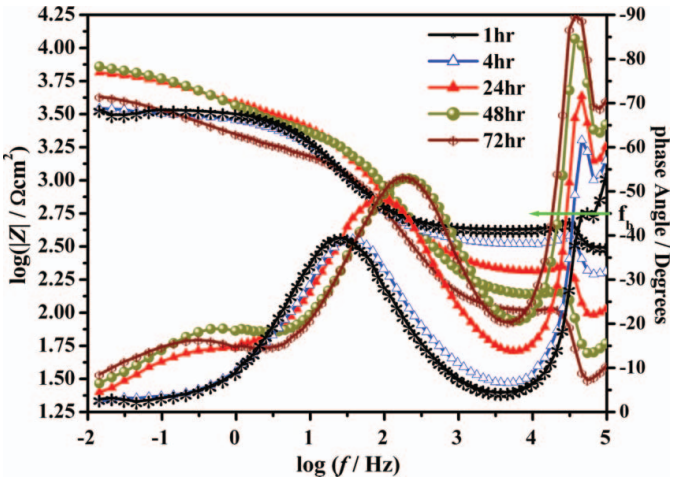

FIG. 4. Bode plot corresponds to Zn-TiO_2 composite coating D_2 (color figure available online).

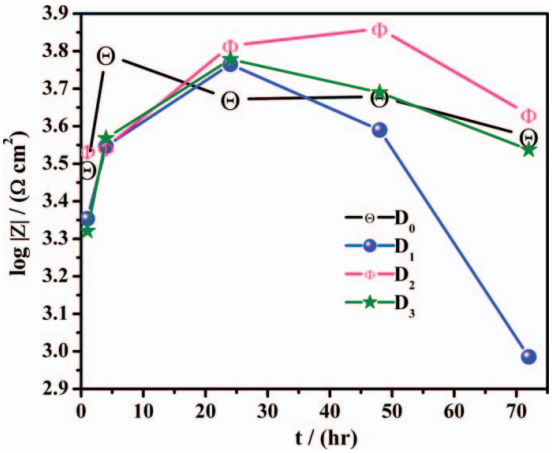

FIG. 5. Total impedance value |Z| with respect to time for Zn coating D_0 and Zn-TiO_2 composite coatings D_1, D_2, and D_3 (color figure available online).

The break point frequency f_b (i.e., the frequency for a 45° phase angle, higher frequencies shift correlated with relative increase of electrochemically active surface area)[24,25] shifted toward lower frequencies with respect to time for all coatings. This suggests that the electroactive surface area decreases with increase in immersion time because of the protective corrosion products layer between electrolyte and coated electrode surface. The f_b shift with respect to time corresponds to D_2 coating is given in Figure 4 and f_b shift in all the coatings at different immersion time is given in Figure 6. For all the coatings, at 1 hr and 4 hr impedance measurements the f_b value is higher than other measurements, because at 1 hr and 4 hr immersion time there is no considerable corrosion products are observed on the electrode surface. But shift in f_b towards low frequency was observed in 24, 48 and 72 hr measurements. According to Figure 6 more f_b shift was observed for coatings D_0 and D_3, but these coatings showed minimum resistance than the coating D_2. This means even though there is maximum surface area coverage for coating D_0 and D_3, which exhibit less corrosion resistance behavior. This may be due to the porous nature of the corrosion product layer and adherent property of that layer. However, D_2 coating shows considerable f_b shift towards low frequency with respect to time along with its anticorrosive nature.

In the present work the AC circuit having parallel R and C combination was employed. Hence, the phase difference arises between current and voltage leads to current flow through either capacitor or resistor. The coating is capacitive if resistance and/or capacitance are high, so the current mostly passes through capacitor and therefore the phase angle would be near –90°. The coating is resistive if resistance and/or capacitance are low, so the current mostly passes through resistor and therefore phase angle would be near 0°.[26,27]

High-frequency response in the Bode plot of phase angle v/s log frequency describes the behavior of coating when it is in contact with corrosive media. As per previous results in the present study, there is no considerable adherent corrosion product at the 1 and 4 h immersion time. So the AC current mostly passes through the resistor, hence phase angle is minimum. After forming adherent corrosion products layer, it separates the coated electrode surface and electrolyte, and hence the current is impeded passing through the resistor and it prefers capacitor to pass through. As a result phase angle at high frequency is close to –90° in the 24, 48, and 72 h immersion period measurements. The variation of phase angle with respect to immersion time for D_2 coating is represented in Figure 4.

In Nyquist plots three relaxation processes were observed and are well resolved in phase angle v/s log frequency Bode plots (Figure 4). In Bode plots, peak corresponds to second time constant is considered as characteristic peak for charge transfer resistance. The R_{ct} characteristic peak for all coating is shifted toward high frequency with respect to immersion time and this shift is given in the Figure 7. This shift shows that as immersion time increases the electron transport between coated layer and

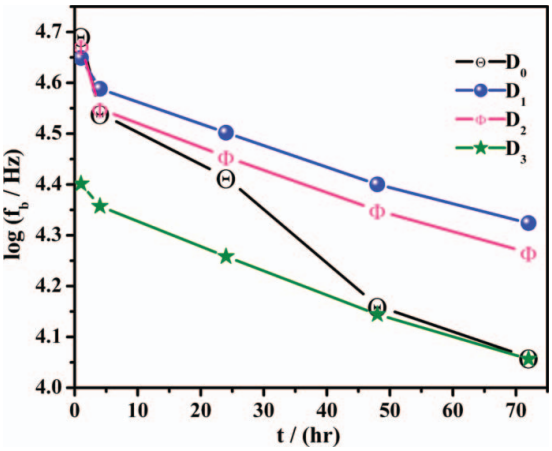

FIG. 6. Break frequency (f_b) value with respect to time for Zn coating D_0 and Zn-TiO_2 composite coatings D_1, D_2, and D_3 (color figure available online).

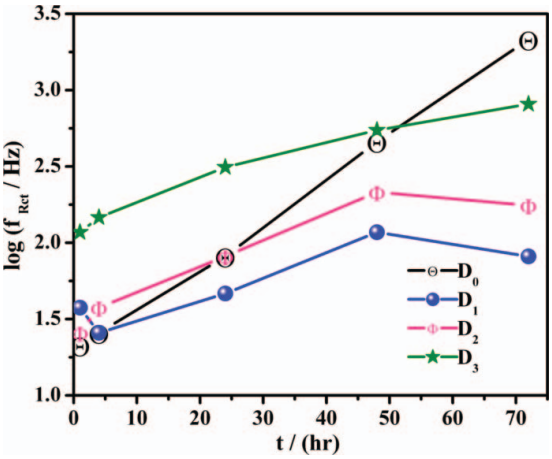

FIG. 7. Charge transfer characteristic frequency (f_{Rct}) with respect to time for Zn coating D_0 and Zn-TiO_2 composite coatings D_1, D_2, and D_3 (color figure available online).

electrolyte may encounter longer distance because of formation of corrosion products protective layer.[28] The coatings D_0 and D_3 showed maximum shift with respect to time even though they possess lower corrosion resistance than D_2 coating. This behavior may be due to the thick corrosion products layer formed because of the rapid corrosion process, but the main protecting ability based on the adherence, thickness, and permeability of the protective layer along with the coated layer response to corrosion kinetics. In spite of these, D_2 coating exhibited good shift along with its anticorrosive property and it is shown in Figure 7.

All the impedance parameters disclose that during long time immersion in corrosive media, the formed corrosion products acts as a protective layer by separating coated layer and electrolyte. But the main impact is from TiO_2 particles because these particles impart good, compact, and uniform deposit by minimizing the dislocations or active sites, which accelerates the corrosion process. Eventually Zn-TiO_2 composite coating, in particular coating generated from the plating bath containing 6 g/L of TiO_2 particles (i.e., D_2), shows good anticorrosive behavior to external aggressive environment.

Surface Characterization

The EDS and SEM micrographs corresponding to Zn and Zn-TiO_2 (D_2) composite coatings are given in Figures 8 and 9. The presence of Ti peak in the EDS spectra confirms that TiO_2 particles are incorporated in Zn matrix during Zn-TiO_2 composite coating process. The percentage of Ti obtained from EDS spectra for the D_1, D_2, and D_3 composite coatings are 0.35%, 0.72%, and 0.43%, respectively.

The SEM micrographs in Figure 9 corresponds to Zn coating and Zn-TiO_2 (D_2) composite coating. In addition to EDS spectra, the SEM image of D_2 also confirms the presence of TiO_2 particles in composite coatings. The SEM images showed similar shape of randomly oriented hexagonal platelets. And the composite coatings showed uniform grains with more compact crystalline structure when compared to pure zinc coating. This reveals that TiO_2 nanoparticles are included in Zn matrix

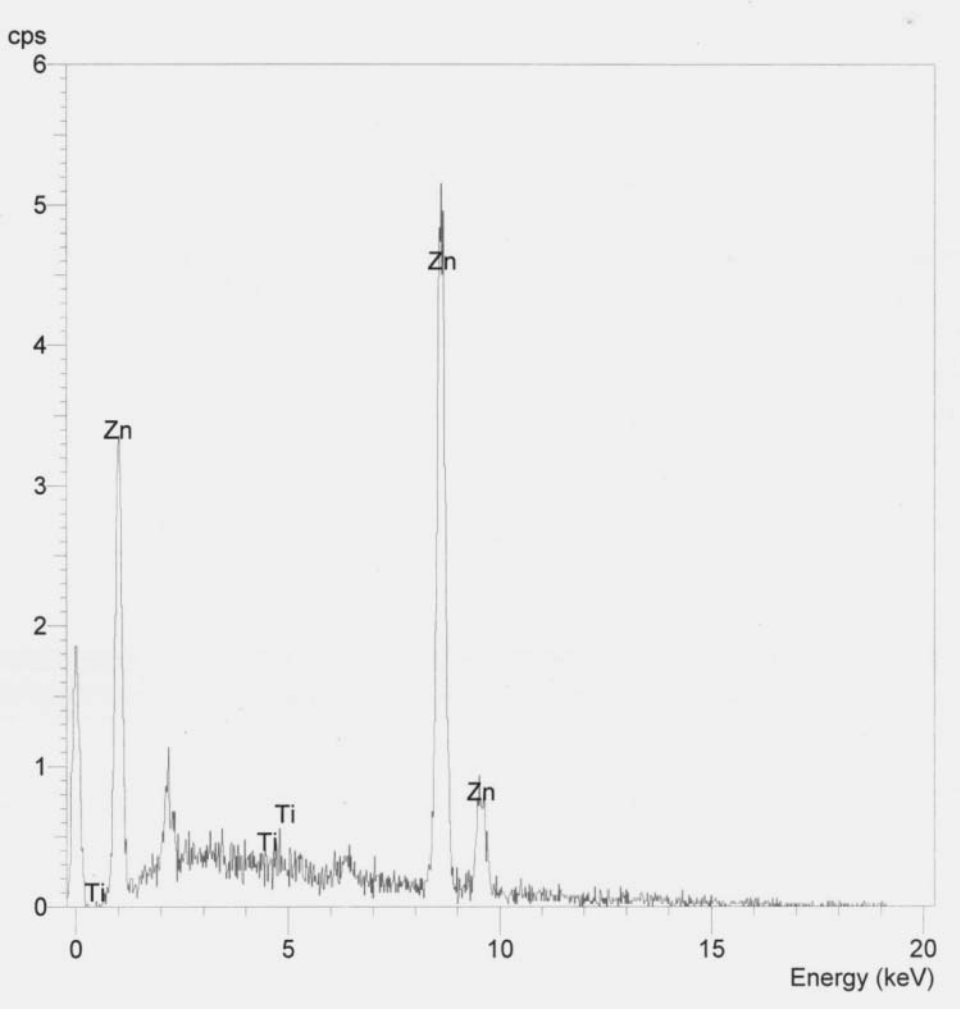

FIG. 8. SEM surface morphology of Zn coating D_0 and Zn-TiO_2 composite coating D_2 (arrow mark shows the presence TiO_2 particles in deposit).

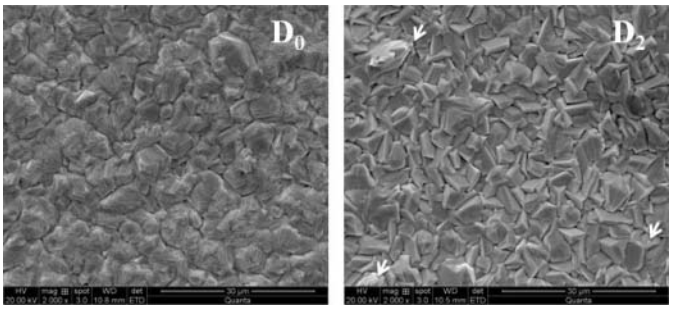

FIG. 9. EDS spectra of Zn-TiO_2 composite coating D_2.

and these particles imparted morphological changes to the zinc deposit.

In the case of composite coating, the incorporation of TiO_2 particles to the Zn matrix bring changes to the average crystal size and orientation of Zn crystal plane and it is observed from recorded XRD patterns (Figure 10) and texture coefficient calculation. The average crystal size calculated from the Scherrer equation (Eq. 2) for pure Zn is 83.62 nm and for composite coating D_1 is 104.58 nm, D_2 is 103.31 nm, and D_3 is 115.06 nm.

$$L = \frac{K\lambda}{\beta \cos\theta} \quad [2]$$

where K is the Scherrer constant, λ is wavelength of scattering, β is full-width half maxima, θ is scattering angle, and L is average crystal size.

It is inferred that the grain size of Zn crystallites are not refined by incorporation of TiO_2 nanoparticles but the nanoparticles made compact arrangement of Zn crystallites, which is also observed in SEM images.

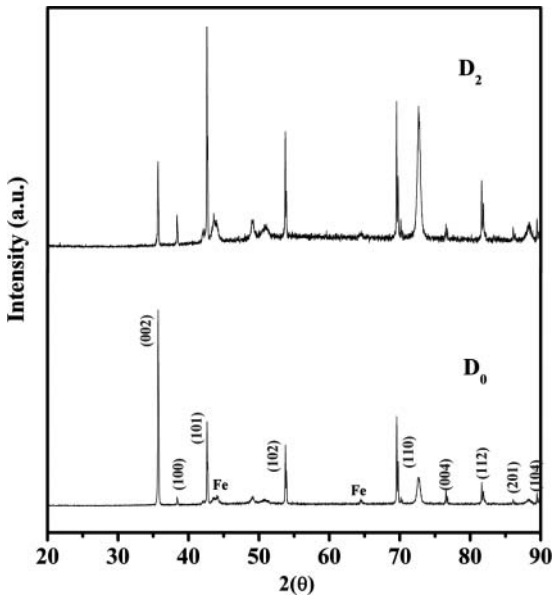

FIG. 10. XRD patterns of Zn coating D_0 and Zn-TiO_2 composite coating D_2.

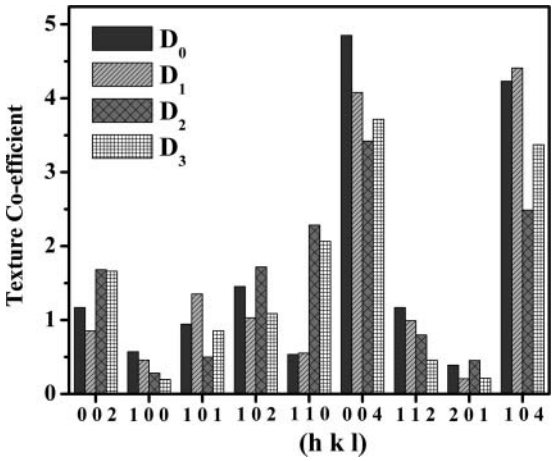

FIG. 11. Preferential orientation of Zn crystallites of Zn coating D_0 and Zn-TiO_2 composite coatings D_1, D_2, and D_3.

The characteristic peak of TiO_2 in composite coating was not observed in the XRD patterns, maybe due to the little content TiO_2 nanoparticles in composite coatings. However, SEM and EDS analysis confirmed the existence of TiO_2 particles in composite coatings.

To know the growth of new crystal plane after the inclusion of TiO_2 particles in Zn deposit, the texture coefficient was calculated from X-ray diffraction patterns. The texture coefficient (Tc) was calculated by using the equation $Tc = [I(hkl)/\sum I(hkl)] \times [\sum IO(hkl)/IO(hkl)]$.[29] Where $I_{(hkl)}$ is the peak intensity of electrodeposits and $\sum I(hkl)$ is the sum of intensities of the independent peaks. And O refers to the standard zinc powder sample. The determined texture coefficient are shown in Figure 11.

The majority of Zn crystallites in pure Zn coating are oriented parallel to the (1 0 0), (0 0 4), and (1 1 2) planes, but in Zn-TiO_2 composite coatings the preferred orientation is changed. Among the composite coatings, D_2 showed intense orientation in (0 0 2), (1 0 2), (1 1 0), and (2 0 1) planes. This change in preferred orientation of Zn crystallite planes in Zn-TiO_2 composite coatings is due to the incorporation of TiO_2 nanoparticles in the Zn matrix. Also the increase in texture intensity in the coating D_2 influences the corrosion behavior of deposit.[30]

The results obtained from different surface characterization studies confirms that during Zn deposition TiO_2 nanoparticles are incorporated in Zn matrix and these incorporated particles have changed the morphology of the Zn deposit and increased the corrosion resistance property of the deposited Zn layer in the case of Zn-TiO_2 composite coatings.

CONCLUSION

The Zn-TiO_2 composite coatings were successfully generated on mild steel from bath solution containing 2, 6, and 10 g/L of rutile TiO_2 nanoparticles. The potential shift toward less negative in Tafel polarization and improved polarization resistance with shift in f_b and Rct characteristic frequency confirmed the anticorrosive behavior of Zn-TiO_2 composite coatings. All

deposits showed corrosion resistant property up to 72 h. The incorporated TiO_2 nanoparticles changed the morphology of Zn crystallites, the average crystal size, and preferred orientation. The preferred orientation of D_2 deposit changed to (0 0 2), (1 0 2), and (1 1 0) from (1 0 0), (0 0 4), and (1 1 2). The higher percentage of TiO_2 content of D_2 provides compact and uniform surface to the D_2 deposit. These morphological changes imported good corrosion resistance property to the deposit D_2.

REFERENCES

1. Prabhu, R.A.; Venkatesha, T.V.; Shanbhag, A.V.; Praveen, B.M.; Kulkarni, G.M.; Kalkhambar, R.G. Quinol-2-thione compounds as corrosion inhibitors for mild steel in acid solution. *Mater. Chem. Phys.* **2008**, *108*, 283–289.
2. Li, J.; Sun, Y.; Sun, X.; Qiao, J. Mechanical and corrosion-resistance performance of Electrodeposited titania-nickel nanocomposite coatings. *Surf. Coat. Technol.* **2005**, *192*, 331–335.
3. Wu, G.; Li, N.; Derui; Mitasuo, K. Electrodeposited Co-Ni-Al_2O_3composite coatings. *Surf. Coat. Technol.* **2004**, *176*, 157–164.
4. Thiemig, D.; Bund, A. Characterization of electrodeposited Ni-TiO_2 nanocomposite coatings. *Surf. Coat. Technol.* **2008**, *202*, 2976–2984.
5. Vathsala, K.; Venkatesha, T.V. Zn–ZrO_2 nanocomposite coatings: elecrodeposition and evaluation of corrosion resistance. *J. Appl. Surf. Sci.* **2011**, *257*, 8929–8936.
6. Praveen. B.M.; Venkatesha, T.V.; Naik, Y.A.; Prashantha, K. Corrosion behavior of Zn-TiO_2 composite coating. *Synth. React. Inorg. Met-Org. Chem.* **2007**, *37*, 461–465.
7. Chandrappa, K.G.; Venkatesha, T.V.; Nayana, K.O.; Punith Kumar, M.K. Generation of nanocrystalline NiO particles by solution combustion method and its Zn–NiO composite coating for corrosion protection. *Mater. Corros.* **2011**, *62*, 1–11.
8. Vlasa, A.; Varavara, S.; Pop, A.; Bulea, C.; Muresan, L.M. Electrodeposited Zn-TiO_2 nanocomposite coatings and their corrosion behavior. *J. Appl. Electrochem.* **2010**, *40*, 1519–1527.
9. Shibli, S.M. A.; Dilimon, V.S.; Smith, P.A.; Manu, R. Incorporation of TiO_2 in hot dip zinc coating for efficient resistance to biogrowth. *Surf. Coat. Technol.* **2006**, *200*, 4791–4796.
10. Miller, L.W.; Tejedor-Tejoder, I.M.; Anderson, M.A. Titanium dioxide-coated silica waveguides for the photocatalytic oxidation of formic acid in water. *Environ. Sci. Technol.* **1999**, *33*, 2070–2075.
11. Sun, B.; Reddy, E.P.; Smirniotis, P.G. Visible light Cr(VI) reduction and organic chemical oxidation by TiO_2 photocatalysis. *Environ. Sci. Technol.* **2005**, *39*, 6251–6259.
12. Linsebigler, A.L.; Lu, G.; Yates, J.T. Jr. Photocatalysis on TiO_2 surface: principles, mechanism and selected results. *Chem. Rev.* **1995**, *95*, 735–758.
13. Yang, X.; Li, Q.; Zhang, S.; Liu, F.; Wang, S.; Zhang, H. Microstructure characteristic and excellent corrosion protection of sealed Zn-TiO_2 composite coatings for sintered NdFeB magnet. *J. Alloys Compd.* **2010**, *495*, 189–195.
14. Gomes, A.; Almeida, I.; Frade, T.; Tavares, A.C. Zn-TiO_2 and ZnNi-TiO_2 nanocomposite coatings: corrosion behaviour. *Mater. Sci. Forum* **2010**, *636–637*, 1079–1083.
15. La Mantia, F.; Vetter, J.; Novak, P. Impedance spectroscopy on porous materials: a general model and application to graphite electrodes of lithium-ion batteries. *Electrochim. Acta* **2008**, *53*, 4109–4121.
16. Zhang, J.-T.; Hu, J.-M.; Zhang, J.-Q.; Cao, C.-N. Studies of water transport behavior and impedance models of epoxy-coated metals in NaCl solutions by EIS. *Prog. Org. Coat.* **2004**, *51*, 145–151.
17. Liu, W.; Zhang, H.; Qu, Z.; Zhang, Y.; Li, J. Corrosion behavior of the steel used as a huge storage tank in seawater. *J. Solid State Electrochem.* **2010**, *14*, 965–973.
18. Macak, J.; Sajdl, P.; Kucera, P.; Novotny, R.; Vosta, J. In situ electrochemical impedance and noise measurements of corroding stainless steel in high temperature water. *Electrochim. Acta* **2006**, *51*, 3566–3577.
19. Mishra, A.K.; Balasubramaniam, R.; Tiwari, S. Corrosion inhibition of 6061-SiC by rare earth chlorides. *Anti-Corros. Met. Mater.* **2007**, *54*, 37–46.
20. Muresan, L.; Varavara, S.; Stupnisek-Lisac, E.; Otmacic, H.; Marusic, K.; Horvat-Kurbegovic, S.; Robbiola, L.; Rahmouni, K.; Takenouti, H. Protection of bronze covered with patina by innoxious organic substances. *Electrochim. Acta* **2007**, *52*, 7770–7779.
21. Dermaj, A.; Hajjaji, N.; Joiret, S.; Rahmouni, K.; Srhiri, A.; Takenouti, H.; Vivier, V. Electrochemical and spectroscopic evidences of corrosion inhibition of bronze by a triazole Derivative. *Electrochim. Acta* **2007**, *52*, 4654–4662.
22. Kinlen, P.J.; Silverman, D.C.; Jeffreys, C.R. Corrosion protection using polyaniline coating formulations. *Synth. Met.* **1997**, *85*, 1327–1332.
23. Epelboin, I.; Keddam, M.; Takenouti, H. Use of impedance measurements for the determination of the instant rate of metal corrosion. *J. Appl. Electrochem.* **1972**, *2*, 71–79.
24. Scully, J.R. Electrochemical impedance of organic-coated steel: correlation of impedance parameters with long-term coating deterioration. *J. Electrochem. Soc.* **1989**, *136*, 979–990.
25. Jianguo, L.; Gaoping, G.; Chuanwei, Y. EIS study of corrosion behaviour of organic coating/dacrometcomposite systems. *Electrochim. Acta* **2005**, *50*, 3320–3332.
26. Mahdavian, M.; Attar, M.M. Investigation on zinc phosphate effectiveness at different pigment volume concentrations via electrochemicalimpedance spectroscopy. *Electrochim. Acta* **2005**, *50*, 4645–4648.
27. Mahdavian, M.; Attar, M.M. Another approach in analysis of paint coatings with EIS measurement: phase angle at high frequencies. *Corros. Sci.* **2006**, *48*, 4152–4157.
28. Hsu, C.-P.; Lee, K.-M.; Huang, J.T.-W.; Lin, C.-Y.; Lee, C.-H.; Wang, L.-P.; Tsai, S.-Y.; Ho, K.-C. EIS analysis on low temperature fabrication of TiO_2 porous films for dye-sensitized solar cells. *Electrochim. Acta* **2008**, *53*, 7514–7522.
29. Fustes, J.; Gomes, A.; da Silva Pereira, M.I. Electrodeposition of Zn-TiO_2 composite films-effect of bath composition. *J. Solid State Electrochem.* **2008**, *12*, 1435–1443.
30. Mouanga, M.; Ricq, L.; Douglade, J.; Bercat, P. Effects of some additives on the corrosion behavior and preferred orientation zinc obtained by continuous current deposition. *J. Appl. Electrochem.* **2007**, *37*, 283–289.